

PACS numbers: 42.79Gn; 42.81.Dp
DOI: 10.1070/QE2003v033n10ABEH002526

Concentration of light energy within a cone with a metal coating

T.I. Kuznetsova, V.S. Lebedev

***Abstract*. The spatial structure of light waves of the electric type in a cone with perfectly reflecting metal walls is theoretically analysed. The exact formulas and asymptotic expressions are derived which describe the dependences of the energy density of different components of the field inside the cone on the radial coordinate. A special attention is paid to the study of the character of the field decrease near the cone apex depending on the cone angle and the wavelength. The effects of reflection of waves from the truncated cone – free space interface are studied. The obtained results are used for calculating the transmission coefficient of a truncated cone in the optical range for a broad range of parameters, including the diameter of the output aperture of the order of 0.05 – 0.1 of the wavelength. The possibility of obtaining a high transmission coefficient of light in a truncated metallised cone is theoretically substantiated.**

Keywords: *near-field optics, nanometer scale, conic waveguide, transmission coefficient, reflection from a subwavelength aperture.*

1. Introduction

A near-field scanning optical microscope is based on the possibility to localise light within a region of subwave size. In this connection, the development of a light source with adequate characteristics is very important problem because only the combination of a high localisation degree with a sufficient energy density can provide the high-quality imaging of nanoobjects.

A number of experimental and theoretical papers devoted to the development of a quasi-point radiation source for probing nanoobjects have been published in recent years. For this purpose, metallised optical fibres tapering to $\lambda/20 - \lambda/10$ at the output are most often used in experiments [1 – 5]. Among the first theoretical studies describing such optical devices are papers [6 – 9]. In [6], an analytic approach was proposed, which can be used in the case of small inclination angles of the waveguide walls. In this case, the transmission coefficient of the waveguide proves to be quite small. In Refs [7 – 9], the method of multiple multipoles [10, 11] was used. This method was applied to calculate the propagation of light through a tapered waveguide with metallised walls and the open end [8] and through a waveguide with a thin metal layer deposited on its output end [9]. In Ref. [8], calculations were performed for the geometry with a weak transmission of light, while in Ref. [9], due to the action of the plasmon mechanism in a metallised waveguide end, the intensity of light at the waveguide output appears to increase.

The idea of using surface waves propagating along metal walls was also developed in Refs [12 – 14]. The authors of these papers combined this approach with the development of a new geometry of a tapered fibre (the so-called double and triple cone, i.e., the presence of the regions in the fibre with different inclination angles of the walls to the fibre axis). As a result, the expected value of the transmission coefficient increased from $10^{-6} - 10^{-5}$ to 10^{-2}. In addition, the transmission coefficient close to 10^{-2} was experimentally observed [14] for small output diameters (70 – 100 nm).

The properties of waves in tapered fibres were approximately analytically described in paper [15], where the transmission coefficients were numerically estimated. Within the framework of the adiabatic approximation (corresponding to a slow variation in the fibre diameter along its axis), the mutual interaction of counterpropagating waves caused by the wall inclination was explicitly taken into account. The interaction of the fundamental waves with the higher-order waves was neglected, and the approximate boundary conditions were used. Such an approach is justified when the wall inclination angle is not too large (when the longitudinal component of the electric field makes a small angle with the waveguide surface). We obtained [16 – 18] the exact system of equations for the field in a tapered metallised waveguide with a subwavelength aperture, in which the waves with all the transverse indices and the interaction between them are considered. This system was used to study in detail the behaviour of waves of the magnetic type in the waveguide and to find and analyse the dependences of the transmission coefficient on the geometrical parameters of the waveguide and the wavelength of light. For waves of the electric type, we managed to obtain only approximate estimates.

As a whole, however, the reliable numerical calculations available in the literature concern a comparatively narrow range of the geometrical parameters of fibres, which does not allow one to determine the ultimate transmission coefficient that can be achieved in metallised fibres. To obtain a more detailed picture concerning the behaviour of waves in tapered fibres, it is important to study fields in a cone. The mathematical apparatus available at present

T.I. Kuznetsova, V.S. Lebedev P.N. Lebedev Physics Institute, Russian Academy of Sciences, Leninskii prosp. 53, 119991 Moscow, Russia; e-mail: tkuzn@maill.lebedev.ru, vlebedev@maill.lebedev.ru

Received 14 January 2003
Kvantovaya Elektronika **33** (10) 931 – 937 (2003)
Translated by M.N. Sapozhnikov

allows us to separate eigenwaves corresponding to a cone, i.e., the problem is not complicated by the transfer of the energy of the chosen wave to other modes. In this case, we can investigate rigorously the waves of the magnetic and electric types.

In this paper, we restrict ourselves to the consideration of a cone with perfectly reflecting metal walls in order to obtain, for a sufficiently simple system admitting an exact solution, the rigorous and detailed picture of the behaviour of waves in tapered optical fibres. For definiteness, we will study the fundamental wave of the electric type. We will show that high energy densities of the field can be achieved near the cone apex. A great part of the paper is devoted to the study of a truncated cone. We found that, in the optical range, for the geometrical parameters of the cone under study, the presence of the open end of the waveguide weakly changes the energy density of the fields calculated for closed cone. This will allow us to claim that a simple conic geometry can provide high transmission coefficients even when the output aperture is rather small.

2. Basic equations

Consider a circular cone with the cone angle θ_0. The dielectric constant ε inside the cone is constant and is not equal to unity. We assume that the cone surface is covered by a layer of an ideal metal. This leads to the zero tangential component of the electric field on the cone surface. Let r, θ, and φ be the distance from the cone apex, the polar angle, and the azimuthal angle, respectively. Consider a monochromatic dependence $\exp(-\mathrm{i}\omega t)$ of the fields on time, which will be omitted below for brevity. By using the Hertz function for the electromagnetic field, we have

$$\frac{\partial^2 U}{\partial r^2}+\frac{1}{r^2}\left[\frac{1}{\sin\theta}\frac{\partial}{\partial\theta}\left(\sin\theta\frac{\partial U}{\partial\theta}\right)+\frac{1}{\sin^2\theta}\frac{\partial^2 U}{\partial\varphi^2}\right]+\frac{\omega^2\varepsilon}{c^2}U=0. \tag{1}$$

Let us represent the expressions for the field components in terms of the Hertz function [19]. The subscripts at the components of the fields $\boldsymbol{E}$ and $\boldsymbol{H}$ denote projections to the corresponding axes of the spherical coordinate system. The fields for the waves of the electric type have the form

$$E_r=\frac{\partial^2 U}{\partial r^2}+\frac{\omega^2\varepsilon}{c^2}U,\quad E_\theta=\frac{1}{r}\frac{\partial^2 U}{\partial r\partial\theta},\quad E_\varphi=\frac{1}{r\sin\theta}\frac{\partial^2 U}{\partial r\partial\varphi}, \tag{2}$$

$$H_r=0,\quad H_\theta=-\frac{\mathrm{i}\omega\varepsilon}{c}\frac{1}{r\sin\theta}\frac{\partial U}{\partial\varphi},\quad H_\varphi=\frac{\mathrm{i}\omega\varepsilon}{c}\frac{1}{r}\frac{\partial U}{\partial\theta}. \tag{3}$$

The boundary condition has the form $U(\theta_0)=0$ and provides the equality of the tangential components of the electric field to zero: $E_r(\theta_0)=0$, $E_\varphi(\theta_0)=0$. Recall that θ_0 is the polar angle on the cone surface, i.e., $2\theta_0$ is the cone-opening angle.

In the case of the magnetic type waves, the Hertz function satisfies equation (1). The relation between the fields (with the subscript m) and the Hertz function can be obtained from (2) and (3) after the replacement $E_j\to H_j^{(\mathrm{m})}$ and $H_j\to\varepsilon E_j^{(\mathrm{m})}$. The boundary condition for the magnetic type waves has the form $\partial U/\partial\theta|_{\theta=\theta_0}=0$ and provides the equality of the tangential component of the electric field on the cone surface to zero: $E_\varphi^{(\mathrm{m})}(\theta_0)=0$.

The method of separation of variables gives for equation (1) the solution in the form

$$U(r,\theta,\varphi)=\mathcal{R}(r)P_\nu^m(\cos\theta)\exp(\mathrm{i}m\varphi),$$
$$\mathcal{R}(r)=C\sqrt{r}J_{\nu+1/2}\left(\frac{\omega\sqrt{\varepsilon}}{c}r\right), \tag{4}$$

where $J_{\nu+1/2}$ is the $\nu+1/2$-order Bessel function and P_ν^m is the adjoint Legendre function [20] of the first kind, power ν, and order m (m is integer). The boundary conditions for the waves of the electric and magnetic types take the form

$$P_\nu^m(\cos\theta_0)=0,\qquad \left.\frac{\partial P_\nu^m(\cos\theta)}{\partial\theta}\right|_{\theta=\theta_0}=0, \tag{5}$$

respectively.

Let us present the results of calculations of the lowest eigenvalues for the E-wave with $m=0$ and for the H-waves with $m=0$ and $m=1$ for different cone angles. These waves penetrate through a tapered waveguide more efficiently than higher-order waves (similarly to the results obtained for a cylindrical waveguide). The results of our calculations are presented in Table 1. One can see that an increase in the cone angle $2\theta_0$ leads to a drastic decrease in the lowest eigenvalues ν_1 for all the three types of the eigenwaves in a tapered waveguide. This means that at large θ_0 the waves will penetrate more efficiently through a tapered waveguide. At the same time, when he angle θ_0 is specified, the values of ν_1 for the waves of the electric and magnetic types are substantially different. To obtain a lower spatial decay of the field at the output of a truncated cone, it is preferable to use electric type waves with the azimuthal wave number $m=0$ and magnetic type waves with $m=1$. Below, we will consider only the electric type wave with $m=0$.

Table 1. Lowest eigenvalues ν_1 for the E- and H-waves for different angles θ_0 ($2\theta_0$ is the cone angle).

Wave type	m	θ_0/rad					
		$\pi/24$	$\pi/12$	$\pi/6$	$\pi/4$	$\pi/3$	$\pi/2$
E	0	17.869	8.681	4.083	2.548	1.777	1
H	0	28.776	14.147	6.835	4.405	3.196	2
H	1	13.591	6.584	3.120	2.000	1.468	1

3. Radial dependences of the electromagnetic energy density in a cone

In the case of the electric type wave with $m=0$, the three field components will be nonzero [see (2)–(4)]:

$$E_r=\frac{\nu(\nu+1)}{r^2}\mathcal{R}(r)P_\nu(\cos\theta),\quad E_\theta=\frac{1}{r}\frac{\partial\mathcal{R}(r)}{\partial r}\frac{\partial P_\nu(\cos\theta)}{\partial\theta},$$
$$H_\varphi=\frac{\mathrm{i}\omega\varepsilon}{c}\frac{\mathcal{R}(r)}{r}\frac{\partial P_\nu(\cos\theta)}{\partial\theta}. \tag{6}$$

Consider the dependence of the squares of these components on the radial coordinate r. For each of the components, we will introduce the quantity corresponding to the time-averaged electromagnetic energy density

$$w_r = \frac{\varepsilon}{8\pi}\left\langle [\mathrm{Re}\{E_r \exp(-\mathrm{i}\omega t)\}]^2 \right\rangle = \frac{\varepsilon}{16\pi}|E_r|^2,$$

$$w_\theta = \frac{\varepsilon}{8\pi}\left\langle [\mathrm{Re}\{E_\theta \exp(-\mathrm{i}\omega t)\}]^2 \right\rangle = \frac{\varepsilon}{16\pi}|E_\theta|^2, \quad (7)$$

$$w_\varphi = \frac{1}{8\pi}\left\langle [\mathrm{Re}\{H_\varphi \exp(-\mathrm{i}\omega t)\}]^2 \right\rangle = \frac{1}{16\pi}|H_\varphi|^2.$$

Let us now introduce the integrals of w_r, w_θ, and w_φ over the part of the spherical surface of radius r enclosed inside the cone

$$W_r = 2\pi r^2 \int_0^{\theta_0} w_r(r,\theta)\sin\theta \mathrm{d}\theta,$$

$$W_\theta = 2\pi r^2 \int_0^{\theta_0} w_\theta(r,\theta)\sin\theta \mathrm{d}\theta, \quad (8)$$

$$W_\varphi = 2\pi r^2 \int_0^{\theta_0} w_\varphi(r,\theta)\sin\theta \mathrm{d}\theta.$$

These quantities allow us to study the dependence of the angle-averaged energy densities for different components of the field on the coordinate r. For $r \to \infty$ and $r \to 0$, we can use the asymptotic expansion of the Bessel function for the fields, which immediately demonstrates the radial dependence of the quantities quadratic in the field. For $r \to \infty$, we have

$$|E_r(r\to\infty)|^2 = \frac{2C^2}{\pi}\frac{c}{\omega\sqrt{\varepsilon}}\frac{[v(v+1)]^2}{r^4}\sin^2\left(\frac{\omega\sqrt{\varepsilon}}{c}r - \frac{\pi}{2}v\right) \times [P_v(\cos\theta)]^2, \quad (9)$$

$$|E_\theta(r\to\infty)|^2 = \frac{2C^2}{\pi}\frac{\omega\sqrt{\varepsilon}}{c}\frac{1}{r^2}\cos^2\left(\frac{\omega\sqrt{\varepsilon}}{c}r - \frac{\pi}{2}v\right) \times \left[\frac{\partial P_v(\cos\theta)}{\partial\theta}\right]^2, \quad (10)$$

$$|H_\varphi(r\to\infty)|^2 = \frac{2C^2}{\pi}\frac{\omega\varepsilon\sqrt{\varepsilon}}{c}\frac{1}{r^2}\sin^2\left(\frac{\omega\sqrt{\varepsilon}}{c}r - \frac{\pi}{2}v\right) \times \left[\frac{\partial P_v(\cos\theta)}{\partial\theta}\right]^2. \quad (11)$$

The character of the field decay near the cone apex ($r \to 0$) is determined by the expressions

$$|E_r(r\to 0)|^2 = C^2\left(\frac{\omega\sqrt{\varepsilon}}{2c}r\right)^{2v-2}\left(\frac{\omega\sqrt{\varepsilon}}{2c}\right)^3\left[\frac{v(v+1)}{\Gamma(v+3/2)}\right]^2 \times [P_v(\cos\theta)]^2, \quad (12)$$

$$|E_\theta(r\to 0)|^2 = C^2\left(\frac{\omega\sqrt{\varepsilon}}{2c}r\right)^{2v-2}\left(\frac{\omega\sqrt{\varepsilon}}{2c}\right)^3\left[\frac{v+1}{\Gamma(v+3/2)}\right]^2 \times \left[\frac{\partial P_v(\cos\theta)}{\partial\theta}\right]^2, \quad (13)$$

$$|H_\varphi(r\to 0)|^2 = 4\varepsilon C^2\left(\frac{\omega\sqrt{\varepsilon}}{2c}r\right)^{2v}\left(\frac{\omega\sqrt{\varepsilon}}{2c}\right)^3\frac{1}{\Gamma^2(v+3/2)} \times \left[\frac{\partial P_v(\cos\theta)}{\partial\theta}\right]^2. \quad (14)$$

It follows from expressions (12)–(14) that the less intense component at small r is H_φ. At large distance from the cone apex, the component E_r rapidly decreases with increasing r [see (9)–(11)]. Therefore, by introducing the integrated energy density W_{tot} as a sum of all components of the field

$$W_{\mathrm{tot}}(r) = W_r(r) + W_\theta(r) + W_\varphi(r), \quad (15)$$

we will have $W_{\mathrm{tot}}(\infty) = W_\theta(\infty) + W_\varphi(\infty)$ for $r \to \infty$. Using (10) and (11), we obtain

$$W_{\mathrm{tot}}(\infty) = \frac{C^2}{4\pi}\frac{\omega\varepsilon\sqrt{\varepsilon}}{c}\int_0^{\theta_0}\left[\frac{\partial P_v(\cos\theta)}{\partial\theta}\right]^2\sin\theta\mathrm{d}\theta. \quad (16)$$

It is convenient to normalise all the integrated energy densities, i.e., W_r, W_θ and W_φ to (16). We will also consider separately the integrated energy densities for the electric and magnetic components of the field. The corresponding normalised quantities have the form

$$P_r(r) = \frac{W_r(r)}{W_{\mathrm{tot}}(\infty)}, \quad P_\theta(r) = \frac{W_\theta(r)}{W_{\mathrm{tot}}(\infty)}, \quad (17)$$

$$P_{\mathrm{el}}(r) = P_r(r) + P_\theta(r),$$

$$P_{\mathrm{m}}(r) \equiv P_\varphi(r) = \frac{W_\varphi(r)}{W_{\mathrm{tot}}(\infty)}, \quad P_{\mathrm{tot}}(r) = P_{\mathrm{el}}(r) + P_{\mathrm{m}}(r). \quad (18)$$

Figure 1 shows the angle-averaged integrated energy densities for the radial (P_r) and polar (P_θ) components of the electric field in a cone as functions of the coordinate r. Note that the integrated energy density of the radial component P_r becomes small at distances from the cone apex exceeding the wavelength. This corresponds to asymp-

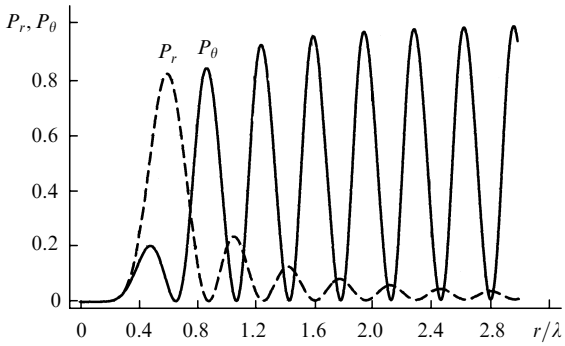

Figure 1. Normalised energy densities of the radial (P_r) and polar (P_θ) components of the electric field in a cone integrated over the spherical surface as functions of the coordinate r measured from the cone apex; $P_r = W_r/W_{\mathrm{tot}}(\infty)$ and $P_\theta = W_\theta/W_{\mathrm{tot}}(\infty)$ are the ratios of the components W_r and W_θ to the integrated total energy density W_{tot} at the waveguide input ($r \to \infty$) for the lowest-order wave ($\lambda = 500$ nm) of the electric type with $m = 0$ ($\varepsilon = 2.25$) and the cone angle $2\theta_0$ ($\theta_0 = \pi/6$, $v_1 = 4.084$).

totic expressions (9)–(11). The dependences of the integrated energy density of the electric field $P_{el} = P_r + P_\theta$ and of the magnetic field $P_m = P_\varphi$ on the coordinate r are presented in Fig. 2. One can see that the curves corresponding to the magnetic and electric energies are out of phase, and at small values of r the integrated energy density of the electric field decays much slower than that of the magnetic field. Figure 2 also shows the dependence of the integrated total energy density $P_{tot} = P_{el} + P_m$ of the electric and magnetic fields in the cone on the coordinate r. According to the normalisation used, the dimensionless quantity P_{tot} rapidly achieves unity (for $r > \lambda$). Note that, as the cone apex is approached, a characteristic peak in observed in the dependence of P_{tot} on r before the beginning of a strong decay. Our calculations show that the intensity of this peak substantially depends on the cone angle, increasing at small angles.

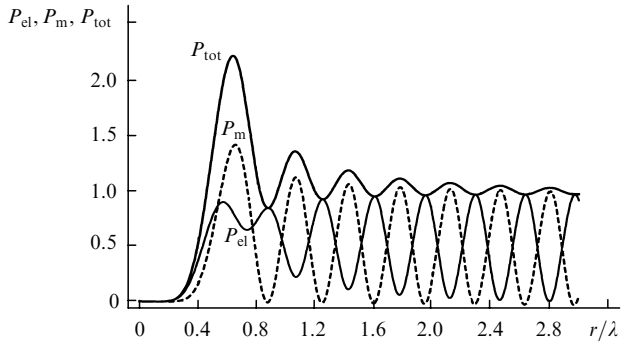

Figure 2. Same as in Fig. 1 for the integrated electric ($P_{el} = P_r + P_\theta$, solid curve) and magnetic [$P_m(r) \equiv P_\varphi(r)$, dashed curve] energy densities. The upper curve is the dependence of the integrated density $P_{tot} = P_{el} + P_m$ on the coordinate r taking into account the contributions from the electric and magnetic fields.

4. Effects of reflection from the truncated cone–free space interface

We considered above the properties of electromagnetic waves in an unperturbed cone. Under real conditions, a cone should be truncated, i.e., its part near the apex should be removed. In the calculation of the energy density of the field at the output aperture of subwave diameter in the zero-order approximation, we can assume that in this case the field structure does not change. Actually, however, the field varies, and we will estimate the scale of perturbations produced upon the cone truncation.

We assume that a part of the cone is cut off by a plane perpendicular to the optical axis. Let us introduce the cylindrical coordinate system (ρ, φ, z) so that the point $(\rho = 0,\ z = 0)$ coincides with the centre of the spherical system $(r = 0)$. Let the plane cutting off the cone apex be described by the equation $z = z_0$. The radius of the output aperture is $a = z_0 \tan\theta_0$. Let us assume that a perfectly conducting surface is located at $\rho > a$, $z = z_0$ (the cone turns to a flange going to infinity). The problem is to match at the aperture the fields in the cone the fields in the free space. To solve this problem rigorously, it is necessary to represent the field in the cone by an infinite superposition of different eigenwaves, and the field in the free space by a continuous set of cylindrically symmetric waves. Let us represent the Hertz function in the form

$$U^{(c)} = C\sqrt{r}J_{\nu+1/2}\left(\frac{\omega\sqrt{\varepsilon}}{c}r\right)P_\nu(\cos\theta) + \sum_{n=1}^{\infty} C_n\sqrt{r}H^{(1)}_{\nu_n+1/2}\left(\frac{\omega\sqrt{\varepsilon}}{c}r\right)P_{\nu_n}(\cos\theta). \quad (19)$$

Expression (19) contains the waves with all the possible eigenvalues (ν_1 coincides with ν). For all $\nu_n \neq \nu$, only the waves going away from the centre are taken because only the wave with $\nu_n = \nu$ is incident on the cone. All the components of the fields in the cone should be now expressed in terms of the new Hertz function (19) with the help of previous formulas [see (2), (3), (6)], in which the quantities E_r, E_θ, H_φ, and U should be replaced by $E_r^{(c)}$, $E_\theta^{(c)}$, $H_\varphi^{(c)}$, and $U^{(c)}$. We should pass now from the fields $E_r^{(c)}$ and $E_\theta^{(c)}$ to the components $E_\rho^{(c)}$ и $E_z^{(c)}$ using the relations

$$E_\rho^{(c)} = E_r^{(c)}\sin\theta + E_\theta^{(c)}\cos\theta,$$

$$E_z^{(c)} = E_r^{(c)}\cos\theta - E_\theta^{(c)}\sin\theta. \quad (20)$$

Let us introduce the special notation

$$\phi(\rho) = E_\rho^{(c)}\left(r = (\rho^2 + z_0^2)^{1/2}, \cos\theta = \frac{z_0}{(\rho^2 + z_0^2)^{1/2}}\right), \quad (21)$$

$$\psi(\rho) = E_z^{(c)}\left(r = (\rho^2 + z_0^2)^{1/2}, \cos\theta = \frac{z_0}{(\rho^2 + z_0^2)^{1/2}}\right) \quad (22)$$

for the values of these fields at the exit hole. The components of the field in the free space are denoted by $E_\rho^{(0)}$ and $E_z^{(0)}$.

At the truncated cone–free space interface, the continuity conditions should be satisfied for the tangential component of the electric field and the normal component of the electric induction

$$E_\rho^{(0)} = E_\rho^{(c)}, \quad E_z^{(0)} = \varepsilon E_z^{(c)} \quad (z = z_0,\ 0 \leqslant \rho < a). \quad (23)$$

In addition, because of the perfect conductivity of the flange, the condition

$$E_\rho^{(0)} = 0 \quad (z = z_0,\ \rho > a) \quad (24)$$

should be fulfilled.

Let us represent the field $E_z^{(0)}$ by the Fourier–Bessel integral with the expansion coefficient $A(\varkappa)$

$$E_z^{(0)}(\rho, z) = \int_0^\infty A(\varkappa)J_0(\varkappa\rho) \times \exp\left[-\mathrm{i}\left(\omega^2/c^2 - \varkappa^2\right)^{1/2}(z - z_0)\right]\varkappa\mathrm{d}\varkappa, \quad (25)$$

where $\varkappa$ is a continuous variable. This dependence on z follows from the Helmholtz equation, to which the component $E_z^{(0)}$ should satisfy. Note that for $\varkappa^2 > \omega^2/c^2$, the factor $-\mathrm{i}(\omega^2/c^2 - \varkappa^2)^{1/2}$ in (25) and all similar expressions should be replaced by $(\varkappa^2 - \omega^2/c^2)^{1/2}$. Such a choice of the radical sign is determined by the requirement that each of the field components $E_z^{(0)}$ was either the wave going away to $-\infty$ (i.e, from the cone) or the wave decaying at $-\infty$.

By calculating $\partial E_z^{(0)}/\partial z$ by means of (25) and using the

condition $\operatorname{div} \boldsymbol{E}^{(0)} = 0$, we obtain

$$-\frac{1}{\rho}\frac{\partial}{\partial\rho}\left(\rho E_\rho^{(0)}\right) = \frac{\partial E_z^{(0)}}{\partial z} = \int_0^\infty \left[-\mathrm{i}\left(\omega^2/c^2 - \varkappa^2\right)^{1/2}\right]$$

$$\times A(\varkappa) J_0(\varkappa\rho) \exp\left[-\mathrm{i}\left(\omega^2/c^2 - \varkappa^2\right)^{1/2}(z - z_0)\right]\varkappa \mathrm{d}\varkappa. \quad (26)$$

In addition, it follows from relations (21), (23), and (24) that

$$-\frac{1}{\rho}\frac{\partial}{\partial\rho}\left(\rho E_\rho^{(0)}\right)\Big|_{z=z_0} = \begin{cases} -\dfrac{1}{\rho}\dfrac{\partial}{\partial\rho}[\rho\phi(\rho)] & (0 \leqslant \rho < a), \\ 0 & (\rho > a). \end{cases} \quad (27)$$

From this we find the expression for the Fourier–Bessel expansion coefficient

$$A(\varkappa) = \frac{-1}{-\mathrm{i}(\omega^2/c^2 - \varkappa^2)^{1/2}} \int_0^a \frac{\partial}{\partial\rho'}[\rho'\phi(\rho')] J_0(\varkappa\rho')\mathrm{d}\rho'. \quad (28)$$

After that, we find from (25)

$$E_z^{(0)}(\rho, z) = -\int_0^\infty \frac{J_0(\varkappa\rho)}{-\mathrm{i}(\omega^2/c^2 - \varkappa^2)^{1/2}}$$

$$\exp\left[-\mathrm{i}\left(\omega^2/c^2 - \varkappa^2\right)^{1/2}(z - z_0)\right]\varkappa \mathrm{d}\varkappa$$

$$\times \int_0^a \frac{\partial}{\partial\rho'}[\rho'\phi(\rho')] J_0(\varkappa\rho')\mathrm{d}\rho'. \quad (29)$$

Assuming then that $z = z_0$ and changing the integration order in (29), we obtain

$$E_z^{(0)}(\rho)\big|_{z=z_0} = -\int_0^a \frac{\partial}{\partial\rho'}[\rho'\phi(\rho')]\mathrm{d}\rho'$$

$$\times \int_0^\infty \frac{J_0(\varkappa\rho) J_0(\varkappa\rho')\varkappa \mathrm{d}\varkappa}{-\mathrm{i}(\omega^2/c^2 - \varkappa^2)^{1/2}}. \quad (30)$$

Using the recurrent relations for cylindrical functions and making the replacement $\varkappa\rho' J_0(\varkappa\rho') = \partial[\rho' J_1(\varkappa\rho')]/\partial\rho'$ in the integrand, we can write (30) in the form

$$E_z^{(0)}(\rho)\big|_{z=z_0} = -\int_0^a \left\{\frac{\partial}{\partial\rho'}[\rho'\phi(\rho')]\right\}$$

$$\times\left\{\frac{1}{\rho'}\frac{\partial}{\partial\rho'}[\rho' L(\rho, \rho')]\right\}\mathrm{d}\rho', \quad (31)$$

$$L(\rho, \rho') = \int_0^\infty \frac{J_0(\varkappa\rho) J_1(\varkappa\rho')\mathrm{d}\varkappa}{-\mathrm{i}(\omega^2/c^2 - \varkappa^2)^{1/2}}. \quad (32)$$

By integrating by parts, we obtain from (31)

$$E_z^{(0)}(\rho)\big|_{z=z_0} = -\left\{\frac{\partial}{\partial\rho'}[\rho'\phi(\rho')] L(\rho, \rho')\right\}\Big|_{\rho'=a}$$

$$+\int_0^a \frac{\partial}{\partial\rho'}\left\{\frac{1}{\rho'}\frac{\partial}{\partial\rho'}[\rho'\phi(\rho')]\right\} L(\rho, \rho')\rho'\mathrm{d}\rho'. \quad (33)$$

Let us rewrite (33) in the form $E_z^{(0)}|_{z=z_0} = \hat{\mathcal{L}}\phi(\rho)$, where the operator $\hat{\mathcal{L}}$ is determined by relations (32) and (33). By substituting this expression into the left-hand side of the second boundary condition in (23) and the field $E_z^{(\mathrm{c})}|_{z=z_0}$, calculated directly from the field $E_r^{(\mathrm{c})}$ and $E_\theta^{(\mathrm{c})}$ in the cone, into its right-hand side, we obtain

$$\chi(\rho) \equiv \hat{\mathcal{L}}\phi(\rho) \equiv \varepsilon\psi(\rho). \quad (34)$$

This equation contains the coefficients C and C_n ($n = 1, 2, \ldots, \infty$), which should be determined and for which system of linear equations can be obtained from (33). Let us assume that the coefficient C_1 is the largest of all the coefficients C_n and discard all of them. Using this simplification, we can represent the Hertz function in the form

$$U^{(\mathrm{c})} = C\sqrt{r}\left[(1 + \beta) J_{\nu+1/2}\left(\frac{\omega\sqrt{\varepsilon}}{c} r\right) + \mathrm{i}\beta Y_{\nu+1/2}\left(\frac{\omega\sqrt{\varepsilon}}{c} r\right)\right]$$

$$\times P_\nu(\cos\theta) \equiv C\sqrt{r}\left[\frac{1}{2} H_{\nu+1/2}^{(2)}\left(\frac{\omega\sqrt{\varepsilon}}{c} r\right)\right.$$

$$\left. + \frac{1 + 2\beta}{2} H_{\nu+1/2}^{(1)}\left(\frac{\omega\sqrt{\varepsilon}}{c} r\right)\right] P_\nu(\cos\theta). \quad (35)$$

Here, $Y_{\nu+1/2}(x)$ is the Neumann function; $H_{\nu+1/2}^{(1)}(x)$ and $H_{\nu+1/2}^{(2)}(x)$ are the Hankel functions of the first and second kinds. This expression contains except a common arbitrary constant a constant $-\beta$, which should be determined. For $\beta = 0$, function (35) is reduced to the previous Hertz function (35) of the cone (1). If the constant β is nonzero, it gives the different amplitudes of the waves coming to the centre and going away from it. It is reasonable to call the ratio of the amplitudes at the functions $H_{\nu+1/2}^{(1)}(x)$ and $H_{\nu+1/2}^{(2)}(x)$ the reflection coefficient R. The value of 2β determines the difference of the reflection coefficient of the truncated cone from unity, i.e.,

$$R = 1 + 2\beta. \quad (36)$$

It is important that the amplitude of the wave coming from $+\infty$ does not vary with β. The algorithm for determining the value of β consists in calculating the fields $E_\rho^{(\mathrm{c})}$, $E_z^{(\mathrm{c})}$, and $E_z^{(0)}$ in the cone and free space and minimising the difference $(E_z^{(\mathrm{c})} - (1/\varepsilon)E_z^{(0)})|_{z=z_0}$ [see the second boundary condition in (23)].

Starting from expression (35) for the Hertz function, with the use of expressions (6) and (20) for the fields in the cone and the first relation in (23), we obtain

$$\phi(\rho) = (1 + \beta)\phi_{\mathrm{B}}(\rho) + \mathrm{i}\beta\phi_{\mathrm{N}}(\rho). \quad (37)$$

In this expression, the separate contributions from the cylindrical Bessel function, $\phi_{\mathrm{B}}(\rho)$, and the cylindrical Neumann function, $\phi_{\mathrm{N}}(\rho)$, to $\phi(\rho)$ are written explicitly. The corresponding combination of the contributions from the Bessel and Neumann functions to the field $E_z^{(0)}|_{z=z_0}$ is calculated from (33). We denote it by $\chi(\rho) = E_z^{(0)}|_{z=z_0}$ and represent in the form

$$\chi(\rho) \equiv (1 + \beta)\chi_{\mathrm{B}}(\rho) + \mathrm{i}\beta\chi_{\mathrm{N}}(\rho), \quad \chi_{\mathrm{B,N}}(\rho) = \hat{\mathcal{L}}\phi_{\mathrm{B,N}}(\rho). \quad (38)$$

The calculation of the field $E_z^{(\mathrm{c})}$ inside the cone also leads to a linear combination of the contributions for the Bessel and Neumann functions. Therefore, the value of $E_z^{(\mathrm{c})}$ at the output aperture [see the second relation in (20)] will have the

form

$$\psi(\rho) = (1+\beta)\psi_{\rm B}(\rho) + {\rm i}\beta\psi_{\rm N}(\rho). \quad (39)$$

The condition for the matching of the z components of the electric fields inside and outside the cone [see the second relation in (23)] will not be satisfied exactly because we have omitted all the highest waves with $\nu_n \neq \nu$ in expression (19). The problem consists in the minimisation of the difference $\psi(\rho) - (1/\varepsilon)\chi(\rho)$. Let us require that the integral

$$I = \int_0^a \left|\psi(\rho) - \frac{1}{\varepsilon}\chi(\rho)\right|^2 \rho {\rm d}\rho \quad (40)$$

would have a minimum, and determine the coefficient β and thereafter R [see (36)].

By substituting (38) and (39) into (40), we obtain

$$I = (1+\beta)(1+\beta^*)I_{\rm B} + \beta\beta^* I_{\rm N} - {\rm i}\beta^*(1+\beta)I_{\rm BN} + {\rm i}\beta(1+\beta^*)I_{\rm BN}^*, \quad (41)$$

$$I_{\rm B} = \int_0^a \left|\psi_{\rm B}(\rho) - \frac{1}{\varepsilon}\chi_{\rm B}(\rho)\right|^2 \rho {\rm d}\rho,$$

$$I_{\rm N} = \int_0^a \left|\psi_{\rm N}(\rho) - \frac{1}{\varepsilon}\chi_{\rm N}(\rho)\right|^2 \rho {\rm d}\rho, \quad (42)$$

$$I_{\rm BN} = \int_0^a \left[\psi_{\rm B}(\rho) - \frac{1}{\varepsilon}\chi_{\rm B}(\rho)\right]\left[\psi_{\rm N}^*(\rho) - \frac{1}{\varepsilon}\chi_{\rm N}^*(\rho)\right]\rho {\rm d}\rho.$$

By differentiating (41) with respect to β^*, we find the condition for the minimum of the quantity I in the form

$$\beta = -\frac{I_{\rm B} - {\rm i}I_{\rm BN}}{I_{\rm B} + I_{\rm N} + {\rm i}(I_{\rm BN}^* - I_{\rm BN})}. \quad (43)$$

We calculated numerically the values of β and found from (36) the corresponding reflection coefficients R (see Table 2) for different values of the output radius a and the cone angle $2\theta_0$. One can see that the reflection coefficient weakly differ from unity in all the cases considered. This means that the solution in the form of the Bessel function (a standing wave in the radial dependence) considered in section 2 is a good approximation for the field in the truncated cone. Note that it was unclear beforehand what relation between the amplitudes of the incoming and outgoing waves [functions $H_{\nu+1/2}^{(2)}$ and $H_{\nu+1/2}^{(1)}$] is adequate to the properties of the open (i.e., truncated) cone.

Table 2. Amplitude reflection coefficient R of light waves at 500 nm on the truncated cone ($\varepsilon = 2.25$) – free space interface and the relative error δ [see (44)] for different values of the angle θ_0 and radius of the output aperture.

a/nm	θ_0/rad	$1 - {\rm Re}\{R\}$	${\rm Im}\{R\}$	δ
12.5	$\pi/12$	2.82×10^{-18}	-7.80×10^{-18}	0.059
	$\pi/6$	2.58×10^{-10}	-8.94×10^{-10}	0.044
	$\pi/4$	7.02×10^{-8}	-3.35×10^{-7}	0.118
	$\pi/3$	4.81×10^{-7}	-3.45×10^{-6}	0.310
25	$\pi/12$	1.65×10^{-12}	-2.52×10^{-12}	0.081
	$\pi/6$	2.76×10^{-7}	-5.20×10^{-7}	0.069
	$\pi/4$	9.17×10^{-6}	-2.36×10^{-5}	0.143
	$\pi/3$	2.22×10^{-5}	-8.61×10^{-5}	0.329
35	$\pi/12$	9.33×10^{-10}	-1.14×10^{-9}	0.108
	$\pi/6$	7.66×10^{-6}	-1.14×10^{-5}	0.101
	$\pi/4$	9.40×10^{-5}	-1.90×10^{-4}	0.173
	$\pi/3$	1.42×10^{-4}	-4.29×10^{-4}	0.353
50	$\pi/12$	6.30×10^{-7}	-6.76×10^{-7}	0.165
	$\pi/6$	2.34×10^{-4}	-2.99×10^{-4}	0.165
	$\pi/4$	1.04×10^{-3}	-1.76×10^{-3}	0.235
	$\pi/3$	1.00×10^{-3}	-2.47×10^{-3}	0.402

The calculations presented above show that the amplitudes of the incoming and outgoing waves are virtually identical for the output radii in the range from zero to $\lambda/10$. We performed calculations not only for the values of the output aperture presented in Table 2 but also for larger values. We found that, for $\lambda = 500$ nm, $\theta_0 = \pi/3$, and $a \sim \lambda/2$, the real part of the amplitude reflection coefficient already strongly differs from unity. Therefore, we can expect that for $a > \lambda/2$, the fields in the closed and truncated cones will be substantially different.

Another question, concerning the form of the field in the truncated cone, is related to the contribution from higher-order waves to the solution. To estimate the error of the solution that neglects the higher-order modes, we estimated the difference between $E_z^{(c)}$ and $(1/\varepsilon)E_z^{(0)}$ at the aperture. To make a rough, knowingly overstated estimate, we took the fields in the zero-order approximation (which do not contain the contribution from the Neumann function). We will consider the average square of this difference divided by the aperture-averaged square of the field calculated for the cone as the relative error δ of the quantities calculated in section 2:

$$\delta = \frac{1}{N_{\rm B}}\int_0^a \left|\psi_{\rm B}(\rho) - \frac{1}{\varepsilon}\chi_{\rm B}(\rho)\right|^2 \rho {\rm d}\rho, \; N_{\rm B} = \int_0^a |\psi_{\rm B}(\rho)|^2 \rho {\rm d}\rho. \quad (44)$$

One can see from Table 2 that the error is small for small cone angles $2\theta_0$. As the angle θ_0 increases, the error also increases and achieves 0.3–0.4 for $\theta_0 = \pi/3$. To calculate reflection more exactly in this case, the contribution from higher-order modes should be taken into account in accordance with the general scheme of calculations outlined in the beginning of this section [see expressions (19)–(34)].

5. Transmission coefficient of a truncated cone with a subwavelength aperture

The transmission coefficient T of a tapered optical fibre is of special interest for applications. We define it as the ratio of the total energy density $P_{\rm tot}^{\rm out} = P_{\rm tot}(r_{\rm out})$ of the field at the output of a truncated cone integrated over the spherical surface $r = r_{\rm out}$, $0 \leqslant \theta \leqslant \theta_0$ to the half the integrated total energy density $P_{\rm tot}^{\rm in} = (1/2)P_{\rm tot}(\infty)$ at the cone input. The factor 1/2 is introduced to take into account the contribution only from the input wave and to exclude the reflected wave. We performed calculations for different values of the output radius a and the angle θ_0, in each case $r_{\rm out} = a/\sin\theta_0$.

Figure 3 shows the dependences of the transmission coefficient T of the truncated cone with the dielectric constant $\varepsilon = 2.25$ on the wavelength λ for the angle $\theta_0 = \pi/6$ and $a = 12.5$, 25, 35, and 50 nm. One can see that, for the specified values of a and θ_0, the transmission

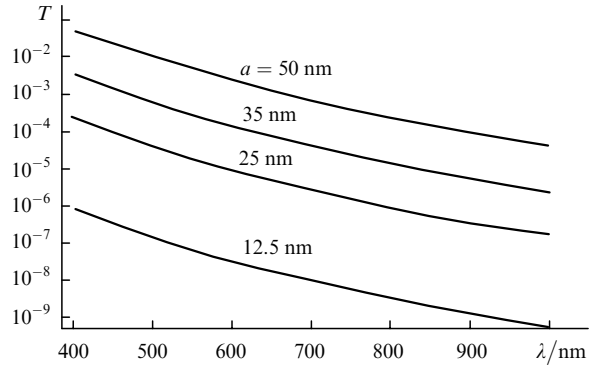

Figure 3. Dependences of the transmission coefficient T of a tapered fibre on the wavelength λ for different values of the output radius a and $\theta_0 = \pi/6$ ($v_1 = 4.084$).

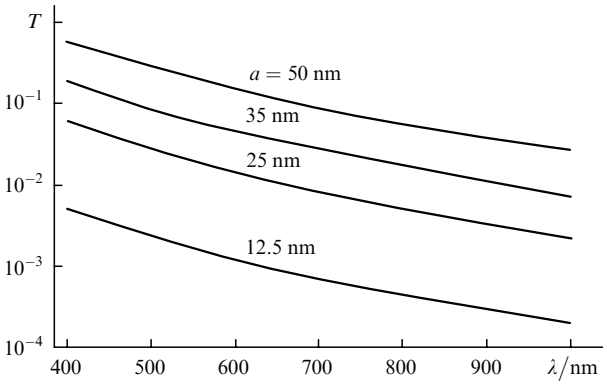

Figure 4. Same as in Fig. 3 but for $\theta_0 = \pi/3$ ($v_1 = 1.777$).

coefficient strongly decreases with increasing λ (it is obvious that short waves are preferable). A decrease in the output radius a leads to a drastic decrease in the transmission coefficient of the fibre. The largest transmission coefficient is obtained for the output radius $a = 50$ nm and is equal to 0.047 and 0.0092 at $\lambda = 400$ and 500 nm, respectively. As the radius was decreases by half ($a = 25$ nm), the transmission coefficient substantially decreased down to 2.4×10^{-4} and 4.1×10^{-5} at the same wavelengths, respectively.

The results of similar calculations of the dependence of the transmission coefficient T on λ for the angle $\theta_0 = \pi/3$ are presented in Fig. 4. Comparison of Figs 3 and 4 shows that the value of T drastically increases with increasing angle θ_0. In particular, for $a = 50$ nm and $\lambda = 400$ and 500 nm, we have $T = 0.56$ and 0.28, respectively for $\theta_0 = \pi/3$ For $a = 25$ nm, we obtain $T = 0.059$ and 0.027 for the same wavelengths, respectively. Therefore, for the same radius of the output aperture, the transmission of a tapered fibre drastically increases compared to the case of $\theta_0 = \pi/6$. Note that a decrease in the transmission coefficient with decreasing output aperture and the inclination angle of the waveguide walls was pointed out earlier [9, 15]. However, this was reliably established only when the transmission of light in the waveguide was rather small. Our study based on the model giving an exact solution allowed us to analyse the case of higher transmission coefficients and to establish the behaviour of the transmission coefficient T for a broad range of geometrical parameters in the entire optical wavelength range.

6. Conclusions

We have analysed the characteristics of light fields in a metallised cone. The dependences of the output radiation intensity on the geometrical parameters of the system are plotted for different variants for the subwavelength output aperture. The effects of reflection of light from the subwavelength aperture of a truncated cone have been considered for the first time. The transmission coefficients of the system under study have been calculated in the optical wavelength range. Our calculations have shown that for $\lambda = 400$ nm, the transmission coefficient can achieve $\sim 0.05 - 0.5$ for the output apertures $2a \approx 50 - 100$ nm and large cone angles ($2\theta_0 = 2\pi/3$).

It follows from the preliminary analysis that, to increase the output radiation intensity in practice, it is necessary to improve the input characteristics of the field (to provide the initially converging wavefront and the symmetric transverse structure) and to reduce reflection at the output with the help of an antireflection coating or some other matching of the output aperture with the characteristics of the free space.

Acknowledgements. This work was supported by the Russian Foundation for Basic Research (Grant Nos 00-02-17245 and 02-02-16274) and the program 'Optical Spectroscopy and Frequency Standards' of the Division of Physical Sciences of the Russian Academy of Sciences.

References

1. Pohl D.W. *Thin Sol. Films*, **264**, 250 (1995).
2. Heinzelmann H., Lacoste Th., Huser Th., Güntherodt H.J., Hecht B., Pohl D.W. *Thin Sol. Films*, **273**, 149 (1996).
3. Islam M.N., Zhao X.K., Said A.A., Mickel S.S., Vail C.F. *Appl. Phys. Lett.*, **71**, 2886 (1997).
4. Eckert R., Freyland J.M., Gersen H., Heinzelmann H., Schürmann G., Noell W., Staufer U., de Rooij N.F. *Appl. Phys. Lett.*, **77**, 3695 (2000).
5. Palanker D.V., Smanovskii D.M., Huie P., Smith T.I. *J. Appl. Phys.*, **88**, 6808 (2000).
6. Roberts A. *J. Appl. Phys.*, **70**, 4045 (1991).
7. Novotny L., Pohl D.W., Regli P. *J. Opt. Soc. Am. A*, **11**, 1768 (1994).
8. Novotny L., Pohl D.W., in *Photons and Local Probes*. Ed by O. Marti, R. Möller (Dordrecht: Kluwer, 1995) p. 21.
9. Novotny L., Pohl D.W., Hecht B. *Opt. Lett.*, **20**, 970 (1995).
10. Hafner Ch. *The Generalized Multiple Multipole Technique for Computational Electromagnetics* (Boston, MS: Artech, 1990).
11. Novotny L., Hafner C. *Phys. Rev. E*, **50**, 4094 (1994).
12. Yatsui T., Kourogi M., Ohtsu M. *Appl. Phys. Lett.*, **71**, 1756 (1997).
13. Yatsui T., Kourogi M., Ohtsu M. *Appl. Phys. Lett.*, **73**, 2090 (1998).
14. Yatsui T., Isumi K., Kourogi M., Ohtsu M. *Appl. Phys. Lett.*, **80**, 2257 (2002).
15. Knoll B., Keilmann F. *Opt. Comm.*, **162**, 177 (1999).
16. Kuznetsova T.I., Lebedev V.S. *J. Russian Laser Research*, **22**, 123 (2001).
17. Kuznetsova T.I., Lebedev V.S. *J. Russian Laser Research*, **23**, 211 (2002).
18. Kuznetsova T.I., Lebedev V.S. *Kvantovaya Elektron.*, **32**, 727 (2002) [*Quantum Electron.*, **32**, 727 (2002)].
19. Vainshtein L.A. *Elektromagnitnye volny* (Electromagnetic Waves) (Moscow: 'Radio i Svyaz', 1988).
20. Abramowitz M., Stegun I.A. (Eds) *Handbook of Mathematical Functions* (New York: Dover, 1965; Moscow: Nauka, 1979).